RESEARCH PAPER

Porous Fe, Co, and N-co-doped carbon nanofibers as high-efficiency oxygen reduction catalysts

Ke Yu · Peng-Hui Shi · Jin-Chen Fan [ID] **· Yu-Lin Min ·
Qun-Jie Xu**

Abstract Oxygen reduction reaction (ORR) is an important reaction in fuel cells. Designing electrocatalysts with outstanding performance is always the key to renewable-energy technologies for fuel cells. Herein, we demonstrate the Fe, Co, and N co-doped porous carbon nanofibers (FeCo/N-C CNFs) as a novel high-performance electrocatalyst for ORR. The synthesis method of this electrocatalysts material is very simple via high-temperature calcination pyrolysis of zinc, cobalt bimetallic zeolitic imidazolate framework (ZIF)-coated electrospun polyacrylonitrile fibers. In alkaline media, the FeCo/N-C CNFs shows a Pt-like ORR performance. The FeCo/N-C CNFs catalysts exhibit excellent performance with an onset potential of 0.99 V and a half-wave potential of 0.83 V in 0.1 M KOH solution, which is similar to those of 20 wt% Pt/C catalysts. Meanwhile, regarding long-term durability and methanol tolerance, the as-synthesized FeCo/N-C CNF catalysts also outperform commercial Pt/C. The unusual catalytic activity mainly from the improvement of electron transfer channels and catalytic sites arise from Fe, Co, and N doping in the porous structure carbon nanofibers.

K. Yu · P.-H. Shi · J.-C. Fan · Y.-L. Min · Q.-J. Xu
Shanghai Key Laboratory of Materials Protection and Advanced Materials in Electric Power, College of Environmental and Chemical Engineering, Shanghai University of Electric Power, Shanghai 200090, China

J.-C. Fan
Department of Chemical Engineering and Biointerfaces Institute, University of Michigan, Ann Arbor, Michigan 48109, USA

P.-H. Shi · J.-C. Fan (✉) · Y.-L. Min · Q.-J. Xu (✉)
Shanghai Institute of Pollution Control and Ecological Security, Shanghai 200092, P.R. China
e-mail: jinchen.fan@shiep.edu.cn
e-mail: xuqunjie@shiep.edu.cn

Introduction

Nowadays, scarcity of fossil resources and deteriorating environment have become two increasingly serious problems. The development and use of sustainable clean energy have become critical. Among them, the fuel cell is a new energy technology that has received extensive attention because of its high efficiency, low pollution, high energy density (Zhu et al. 2015; Wu et al. 2018). Oxygen reduction reaction (ORR) of the fuel cell is a reduction reaction in which oxygen in the cathode of the fuel cell is reacted by a catalyst to obtain electrons. It is a very important electrochemical basic reaction, and it is the most important part of determining the fuel cell rate. Therefore, choosing a good ORR catalyst is a significant task in constructing fuel cell

(Dresselhaus and Thomas 2001; Wang 2005; Qiu et al. 2011). Platinum is a good ORR electrocatalyst. The reaction process is a 4-electron transfer process that does not produce intermediate products. However, the low platinum reserves, the high cost, and the relatively short service life severely restrict the commercial production of fuel cells.

Therefore, to break through these bottlenecks, there are two main research directions in the search for alternative materials to take the place of expensive Pt-based catalysts (Yang et al. 2018). On the one hand, the metal-free heteroatom-doped carbon-based materials exhibit outstanding catalytic performance and favorable long-time stability (Li et al. 2013; Wang et al. 2009; Qu et al. 2010). However, these materials are active only under alkaline media, and their onset potentials are not excellent compared to those of platinum catalyst. Another focus of research is on non-precious metal-based catalysts (Lefevre et al. 2009; Jaouen et al. 2011; Mahmood et al. 2018). Although the onset potentials of these catalysts are almost the same of commercial Pt/C, the stability has always been a difficult problem.

In recent years, considerable attention has been poured into non-precious metal electrocatalysts which display remarkable performance in ORR, consisting of various transition metals species, heteroatom-doped carbon such as N, S, P which can change the electronic distribution of materials, thereby enhancing catalytic performance, and transition metal-nitrogen-doped carbons (M–N–C) (M=Fe, Co, Cu etc.) (Guo et al. 2018). Among them, transition metal-nitrogen-doped carbons are the most promising alternative electrocatalysts, and they have a similar mass activity to Pt/C and outstanding long-time stability. Although a large number of researches infer that the M–N–C plays an important role as an active site (Yang et al. 2018; Hu et al. 2017), the mechanism of ORR active sites in transition metal-nitrogen-doped carbon material has been still uncertain. So far, theoretical calculation and experimental verification have been carried out, and in order to synthesize promising nonprecious metal catalysts (NPMCs) with a Pt-like ORR performance, four critical factors need to be considered: firstly, the number and activity level of the active sites depends on the morphology and composition of the electrocatalyst; secondly, along with the increase of specific surface area and the formation of the pore structure, the degree of exposure of the active site during the oxygen reduction reaction process increases (Jaouen et al. 2011; Liang et al. 2013; Zhang et al. 2018a, b); besides, transition metal coordinated with N element serves as the active site; and finally, the doped heteroatoms (N, S, and B etc.) which are adjacent to the carbon sites change the distribution of electronic structures to enhance the ability to adsorb oxygen (Yang et al. 2017). Based on the above factors, the group of Prof. Baglio has successfully prepared carbon nanofibers modified with a combination of CoO and Co through a simple electrostatic spinning, showing the oxygen catalytic performance with a positive half-wave potential (0.87 V) for ORR (Alegre et al. 2017). Liang et al. have also synthesized a special structure of porous carbon nanofibers (HP-Fe-N/CNFs) via a facile strategy using electrospinning, exhibiting favorable long-time stability with about 87.8% current retention after 10,000 s for ORR (Zhao et al. 2017). Importantly, Fe–Co co-doped porous carbon nanotubes have not yet been reported. It is extremely meaningful via facile electrospinning to synthesize such nanostructured FeCo/N-C as the ORR electrocatalyst for a fuel cell or Zn-air batteries.

Herein, we have successfully synthesized Fe, Co, N co-doped carbon nanofibers (FeCo/N-C CNFs) via a facile method of high-temperature calcination pyrolysis of zinc, cobalt bimetallic zeolitic imidazolate framework (ZIF)-coated electrospun polyacrylonitrile fibers. Because of the addition of zinc acetate in the spinning solution, during the pyrolysis process, the self-etching process can be completed. $Zn(Ac)_2$ and PAN can be respectively pyrolysis to ZnO and carbon at high temperature. After that, ZnO reacts with carbon to make ZnO deplete, thus achieving the purpose of etching carbon nanofibers (Chen et al. 2017). After pyrolysis, the bimetallic ZIF layer will be converted into N-doped porous carbon with high graphitization, and because of self-etching, the carbon nanofibers can form the interconnected hierarchically porous structures. Moreover, the high specific surface area and big pore volume provide electronic transmission channel as well as increase the mass transfer rate and make full use of active sites during the ORR process. Based on the above reasons, the FeCo/N-C CNFs catalysts show promising ORR catalytic performance in alkaline medium. In summary, this catalyst has the potential to be a commercial Pt/C alternative in practical applications.

Experimental section

Materials

Polyacrylonitrile (PAN) powder (average M_w 150,000) was purchased from Shanghai Titan Technology Co. Zinc acetate dehydrate ($Zn(Ac)_2 \cdot 2H_2O$), cobalt(II) acetate tetrahydrate ($Co(Ac)_2 \cdot 4H_2O$) and iron chloride hexahydrate ($FeCl_3 \cdot 6H_2O$) were purchased from Sinopharm Chemical Reagent Co., Ltd. Dimethylformamide (DMF) was purchased from Shanghai Titan Technology Co., Ltd. 2-methylimidazole was purchased from Thermo Fisher Scientific (China) Co., Ltd.

Synthesis of FeCo/N-C CNFs

A total of 2.0 g of PAN powder was first dissolved into 10 mL of DMF with magnetically stirring for 12 h at room temperature (R.T.). Additionally, 1.9 g of $Zn(Ac)_2 \cdot 2H_2O$, 0.1 g of $Co(Ac)_2 \cdot 4H_2O$, and 0.2 g of $FeCl_3 \cdot 6H_2O$ were put into 10 mL DMF to be magnetically stirred together. By then, the obtained $Co(Ac)_2/Zn(Ac)_2/FeCl_3/DMF$ solution was slowly poured into the above PAN/DMF solution under stirring. After continuous mixing overnight, the fully homogeneous mixture solution of $PAN/Co(Ac)_2/Zn(Ac)_2/FeCl_3/DMF$ were obtained and subjected to electrospinning.

For electrospinning, the $PAN/Co(Ac)_2/Zn(Ac)_2/FeCl_3/DMF$ mixture solution was fed into a 10-mL plastic syringe with a 22-gauge stainless steel needle (0.7 * 32 mm). An electrospinning voltage of 15 kV was applied between the needle and the collector. The pushing flow rate of the needle was set as 0.02 mm/min. The rotation speed of the collector was 40 RPM, and the distance between the needle and the collector was set as 20 cm. Afterward, the $PAN/Co(Ac)_2/Zn(Ac)_2/FeCl_3$ composite membranes obtained by electrospinning were directly immersed into 100 mL of 2-methylimidazole/ethanol solution (1 mol/L). After 12 h, $PAN/Co(Ac)_2/Zn(Ac)_2/FeCl_3$ composite membrane was taken out and then washed several times with ethanol. Next, the composite membranes coated with a layer of bimetallic (Co^{2+} and Zn^{2+}) ZIF were dried in an oven for 10 h at 80 °C. Then, for synthesis of FeCo/N-C CNFs, the dried composite membranes were first stabilized under an air atmosphere at 250 °C for 2 h with a heating rate of 1 °C min^{-1} and then carbonized at 800 °C for 20 h in a N_2 flow with a heating rate of 5 °C min^{-1}. In the next, the carbonized membranes were treated in hydrochloric acid (1 M) to remove the residual metal followed with water washing and drying. Finally, the FeCo/N-C CNFs were obtained. For comparison, Fe/N-C CNFs and Co/N-C CNFs were prepared by the same process. The metal contents for FeCo/N-C CNFs, Fe/N-C CNFs, and Co/N-C CNFs were the same by controlling the feed weight and molar ratios before electrospinning.

Instruments and characterization

The morphologies of the samples were observed by scanning electron microscopy (JEOL JSM-7800F) and transmission electron microscopy (JEOL JEM-2100F). The crystal structures were examined by X-ray diffraction (XRD; Bruker D8 advance). Raman spectroscopy was collected by using Lab-RAM HR800 (Horiba Jobin Yvon). Nitrogen adsorption-desorption isotherms and pore-size distribution date were collected using a Micrometrics ASAP2020 analyzer at 77 K. X-ray photoelectron spectroscopy (XPS) were tested with a Kratos Axis UltraDLD spectrometer, using a source gun of Al Kα as the excitation source.

Electrochemical measurements

All the electrochemical measurements were carried out in 0.1 M KOH solution at ambient temperature on a CHI660E electrochemistry workstation with a three-electrode system. A platinum foil was used as counter electrodes, and an Ag/AgCl electrode-saturated KCl was used as reference electrodes. A catalyst film was formed by dropping catalyst ink onto RDE as working electrode. The FeCo/N-C CNFs catalyst ink was prepared by ultrasonically dispersing 4.0 mg of the catalyst powder in a solution containing 800 μL isopropanol, 150 μL deionized water, and 50 μL 0.05wt% Nafion. After that, a certain amount of catalyst ink was added dropwise onto the RDE, giving a catalyst loading of 0.20 mg/cm^2.

All potentials in this study were converted to potentials relative to a reversible hydrogen electrode (RHE) by the following equation:

$$E(\text{vs RHE}) = E(\text{vs } Ag/AgCl) + 0.197 + 0.059pH$$

The electron transfer number during the ORR was determined by the Koutechy-Levich equation:

$$\frac{1}{J} = \frac{1}{J_L} + \frac{1}{J_K} = \frac{1}{B\omega^{1/2}} + \frac{1}{J_K}$$

$$B = 0.2nFC_0D_0^{2/3}\nu^{-1/6}$$

where J, J_L, and J_K are the measured current density and the limiting and kinetic current densities, respectively; ω is the rotating speed, n is the electron transfer number, F is the Faraday constant (96,485 C mol^{-1}), C_0 is the bulk concentration of O_2 (1.2×10^{-3} mol L^{-1}), D_0 is the diffusion coeffcient of O_2 (1.9×10^{-5} cm^2 s^{-1} for 0.1 M KOH solution), and ν is the kinematic viscosity of the electrolyte (0.01 cm^2 s^{-1} for 0.1 M KOH solution).

Results and discussion

As shown in Fig. 1, the preparation process of FeCo/N-C CNFs can be divided into three steps. Firstly, using the $Co(Ac)_2$, $Zn(Ac)_2$, $FeCl_3$, and PAN as start materials, the electrospun nanofiber membranes embedded with metal ions (Co^{2+}, Zn^{2+}, Fe^{3+}) were prepared. Then, the PAN/$Co(Ac)_2$/$Zn(Ac)_2$/$FeCl_3$ composite membranes obtained by electrospinning were directly immersed into 2-methylimidazole/ethanol solution. In this process, some metal ions (Co^{2+} and Zn^{2+}) were continuously dissolved from the inside of the electrospun nanofiber and formed ZnCo-ZIF on the surfaces of nanofibers. Figure 2 a shows the morphologies of PAN/$Co(Ac)_2$/

$Zn(Ac)_2$/$FeCl_3$ composite fibers. The surfaces of the fibers are very clean and smooth. After immersing into the 2-methylimidazole/ethanol solution, the surface morphologies of the fibers obviously changed and became very rough (Fig. 2b). In the meantime, the mean diameter of the fiber obviously increased from ∼ 352.7 to ∼ 444.8 nm with an increase of 92.1 nm. The metal ions (Co^{2+} and Zn^{2+}) dissolved out from the original PAN/$Co(Ac)_2$/$Zn(Ac)_2$/$FeCl_3$ composite fibers and formed ZnCo-ZIF in the presence of the ligand of 2-methylimidazole. After that, the FeCo/N-C CNFs were prepared by carbonization of BM-ZIF@PAN nanofibers at 800 °C for 20 h with N_2 flow. Observing from the SEM images of as-prepared FeCo/N-C CNFs (Fig. 2c), the morphology of the fiber with the mean diameter of ∼ 280 nm is well maintained after carbonization. The shrink in the diameter is mainly due to the volatilization of non-carbon components in PAN during pyrolysis process. TEM images were used to further investigate the structures of FeCo/N-C CNFs. From Fig. 2d–f, it can be clearly seen that the surfaces of FeCo/N-C CNFs exhibit porous fibrous structure derived from BM-ZIF after carbonization with a mean pore size of ∼ 52.75 nm. In fact, the introduction of $Zn(Ac)_2$ can facilitate pore generation due to its self-etching in the process of carbonization. Meantime, the ZnCo-ZIFs covered on the surfaces of fibers turned into the porous carbon frameworks wrapped on the surfaces of nanofibers. Additionally, it is worth noting that there is an individual carbon tube in Fig. 2g growing on the surface of CNFs. It is mainly due to that Fe can be used as catalyst for the
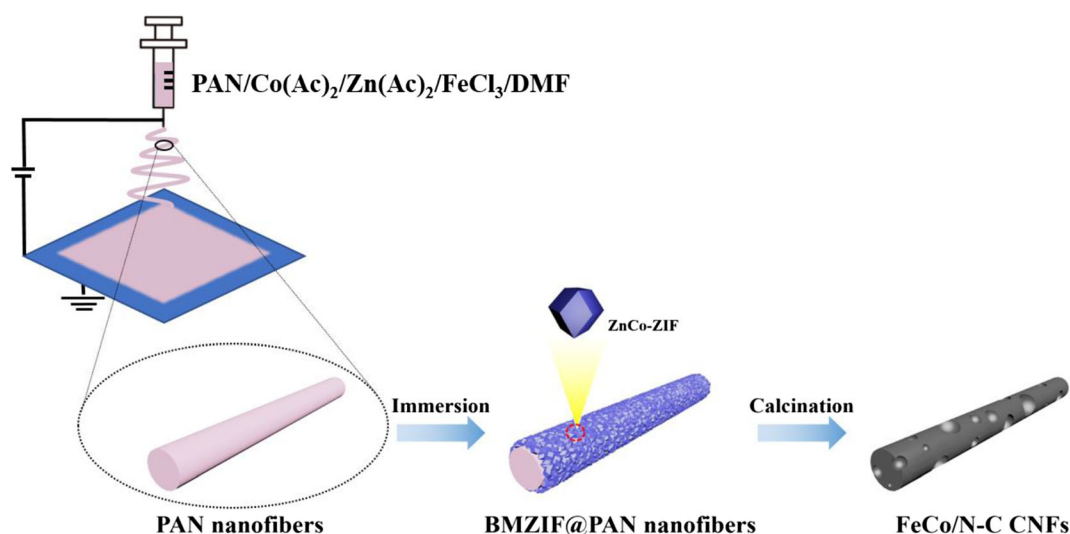
**Fig. 1** Schematic diagram for the preparation process of FeCo/N-C CNFs
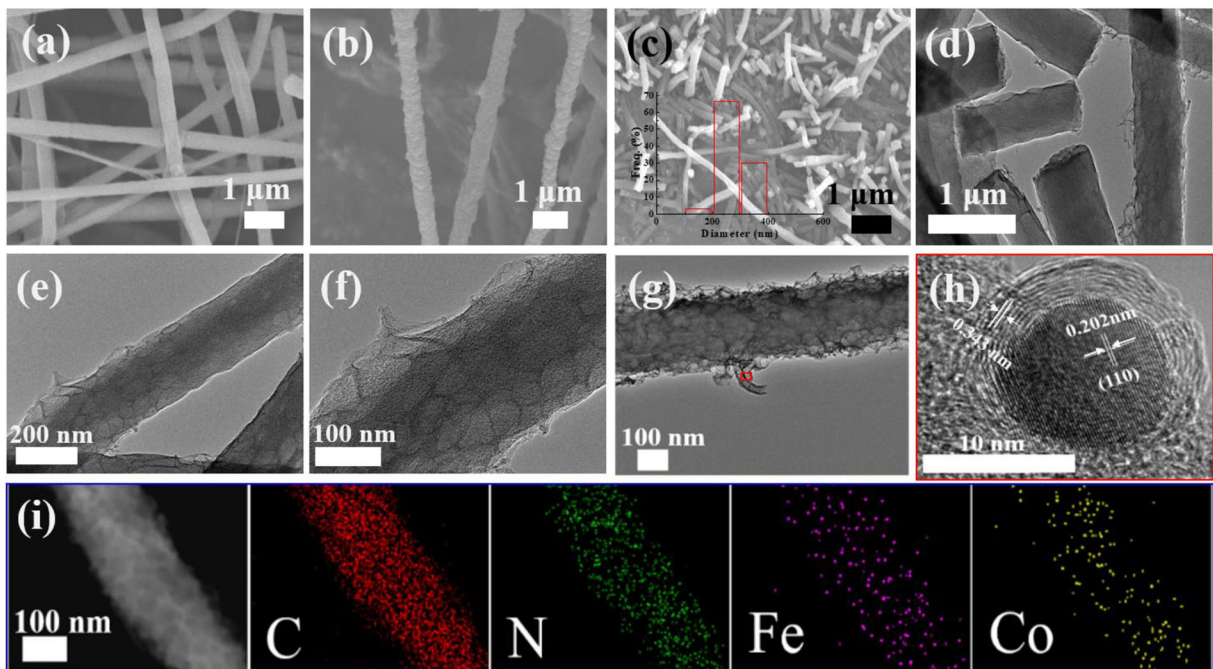
Fig. 2 **a** SEM image of PAN/Co(Ac)$_2$/Zn(Ac)$_2$/FeCl$_3$ nanofibers. **b** SEM image of BM-ZIF@PAN nanofibers, **c** SEM image of FeCo/N-C CNFs. **d**–**g** TEM images of FeCo/N-C CNFs. **f** High-resolution TEM image of FeCo/N-C CNFs. **g** HAADF STEM images and elemental mapping of FeCo/N-C CNFs

formation of carbon nanotubes (Hou et al. 2003; Lee et al. 2002; An et al. 2018). From the HRTEM image, the Fe nanoparticle was encapsulated in the carbon shell with the clear lattice fringe spacing of 0.202 nm corresponding to the (110) planes of Fe (Fig. 2h). The lattice spacing for the outer carbon shell is about 0.343 nm, which is close to that of graphite, 0.34 nm. The Fe NPs wrapped in PAN can catalytically graphitize the carbon precursor to form graphite phase during carbonization process. It is also demonstrated that the Fe and Co doped into the structures of carbon shell did not form nanoparticles anchored on the surfaces of the nanofiber. From the EDS mapping images (Fig. 2i), the elements of nitrogen, iron, and cobalt are well distributed in the FeCo/N-C CNFs. From EDX analysis, the Co and Fe account for about 15.0 wt% and 16.8 wt% of the FeCo/N-C CNFs, respectively.

From Fig. 3a, the diffraction peak at 2θ = 24.6° which is indexed to C (002) crystal plane can be observed in XRD spectra of FeCo/N-C CNFs, Fe/N-C CNFs, and Co/N-C CNFs. The broad peaks at 2θ = 43.8° are originated from the C(100) crystal plane. For FeCo/N-C CNFs, there is a sharp peak located at 2θ = 44.5° and a tiny peak at 2θ = 65.2 which is ascribed to the Fe (110), Fe (200) crystal plane diffraction peak

(JCPDS 87-0722). The crystallite size was determined by using the Debye-Scherrer formula given by $Dhkl = k\lambda/\beta cos\theta$, where D_{hkl} is the crystallite size estimated from the (hkl) line, k is the Scherrer constant, β is the half-width, λ is the X-ray wavelength, and θ is the diffraction angle (Guruvammal et al. 2016). The crystallite size for Fe NPs is ~ 11.135 nm, which is consistent with high-resolution TEM image. Furthermore, Fig. 3b gives the Raman spectra of all the samples to evaluate the degree of graphitization of these catalysts. All spectra of samples show two peaks at about 1350 and 1579 cm^{-1}, which can be attributed to D band representing structural defects and G band representing graphite, respectively (Yang et al. 2015; Shanmugam and Osaka 2011; Lu et al. 2017). The intensity ratios of these two bands (I_D/I_G) of FeCo/N-C CNFs, Fe/N-C CNFs, and Co/N-C CNFs are near ~ 2.1, which reflects the high degree of disorder and defects arise from the dopant of Fe, Co, and N elements. The nitrogen adsorption and desorption isotherm and pore size distribution of FeCo/N-C CNFs are shown in Fig. 3c, d. According to the original IUPAC classification, FeCo/N-C CNFs exhibit type IV isotherms, and its hysteresis loop is clear H4 type hysteresis loops. The total pore volume of FeCo/N-C CNFs is about 115.5 cm^3/g STP estimated
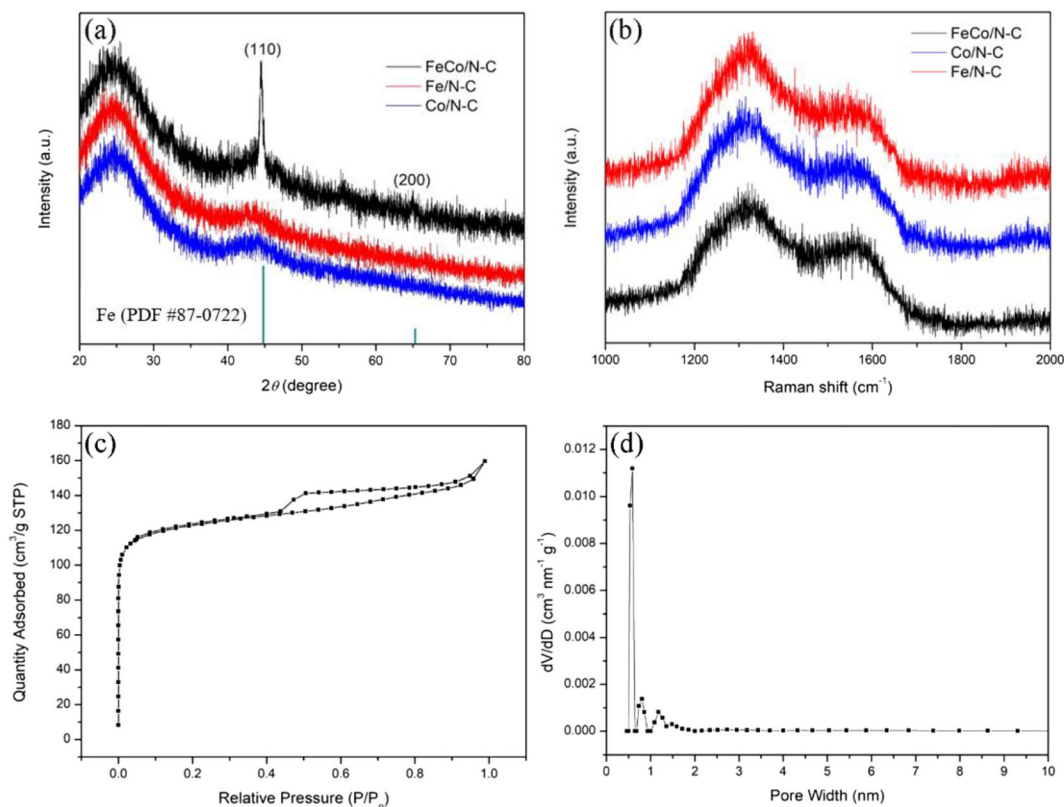
Fig. 3 **a** XRD patterns and **b** Raman spectra of FeCo/N-C CNFs, Fe/N-C CNFs, and Co/N-C CNFs. **c** Nitrogen adsorption-desorption isotherms of FeCo/N-C CNFs. **d** Corresponding pore-size distribution curve of FeCo/N-C CNFs

from the amount adsorbed at $P/P_0 = 0.99$. After converting, the pore volume is about 0.178 cm^3/g STP. Meanwhile, the specific surface area is calculated to be 370.8 $m^2 g^{-1}$. Also, the FeCo/N-C CNFs catalyst has a microspore structure with size distribution concentrate on ~ 1 nm. Therefore, FeCo/N-C CNFs had the rational micropore structure with a large specific surface area, which was beneficial to the mass transport of ORR relevant species and more active sites exposed.

Moreover, the elemental chemical composition and binding energy of the FeCo/N-C CNFs were provided by the X-ray photoelectron spectroscopy (XPS). As shown in Fig. 4a, the spectrum proved the coexistence of C, N, O, Fe, and Co elements in FeCo/N-C CNFs. As exhibited in Fig. 4b, the high-resolution Co 2p XPS spectra exhibited three prominent bands at binding energies of 779.4/794.6, 781.6/796.6, and 786.7/802.9 eV; these peaks can prove the existence of metallic Co, CoC_xN_y, and Co-N_y, Co-O, respectively (Deng et al. 2013; Jiang et al. 2013; Zhang et al. 2018a, b). The peak binding

energies at 781.6/796.6 eV which had two extra peaks located at 786.7/802.9 eV called satellite peak reveal the oxidized Co species (Zhang et al. 2016). Meanwhile, the high-resolution Fe 2p XPS spectra shown in Fig. 4c were deconvoluted into three distinct peaks. Zero-valent Fe (Fe^0) corresponded to the peak located at 706.6 eV, which confirmed the presence of metallic Fe. The other two peaks at 709.7 and 713.4 eV could be ascribed to the $2p_{3/2}$ orbitals of Fe^{2+} and Fe^{3+} species, respectively. Moreover, the shake-up satellite of 718.0 eV also confirmed the presence of Fe^{3+} species (An et al. 2018; Lin et al. 2014; Guan et al. 2018; Peng et al. 2013; Singh et al. 2015; Su et al. 2017; Yamashita and Hayes 2008). Furthermore, the high-resolution N 1s XPS spectra (Fig. 4d) displays four types of peaks: pyridinic-N (398.4 eV), pyrrolic-N (399.7 eV), graphitic-N (400.9 eV), and oxidized-N (403.4 eV) (Lin et al. 2014; Liu et al. 2010; Chen et al. 2015). Also, pyridinic-N bonded to two carbon atoms at the edge of the graphite plane can provide a lone pair of
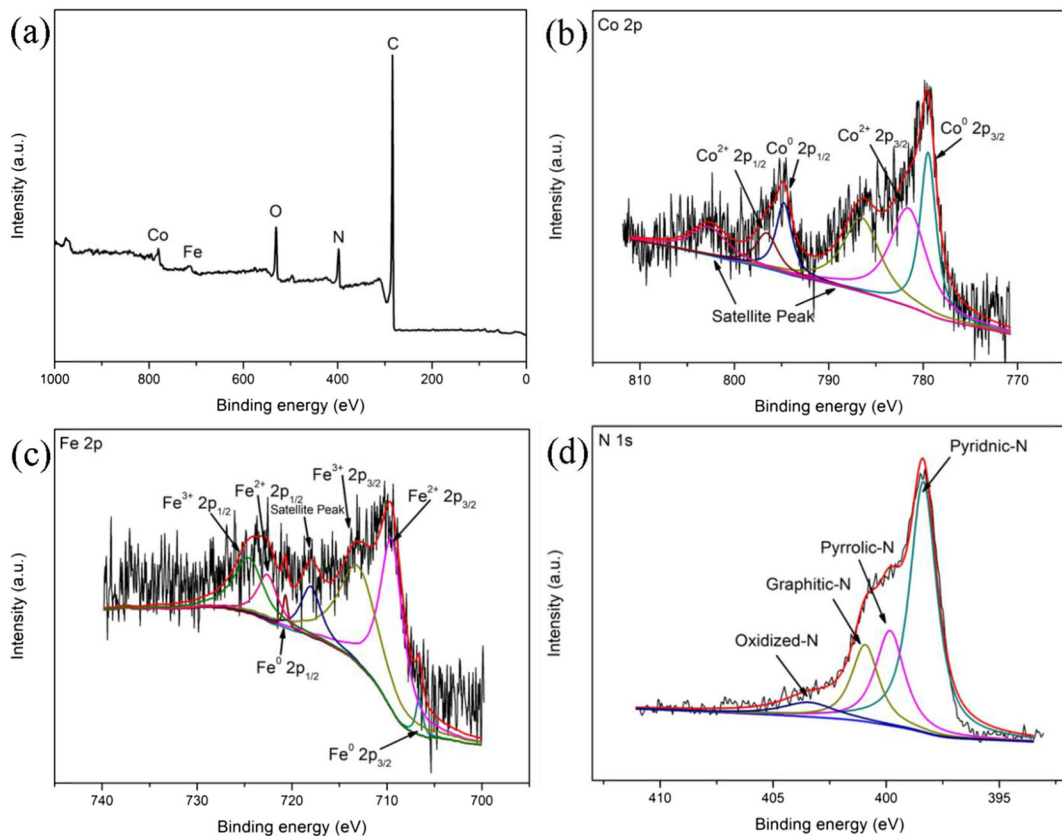
Fig. 4 **a** XPS survey spectrum of FeCo/N-C CNFs. **b** High-resolution of Co 2p, **c** Fe 2p, and **d** N 1s XPS spectrum

electrons and therefore can absorb oxygen and intermediate molecules. And graphitic-N bonded to three carbon atoms in the graphite plane is conducive to raising the limiting current density. So, these two types of N have great influence on ORR activity. Besides, owing to pyridinic-N having electron-donating properties, Fe and Co atoms can be more easily anchored on the material (Lin et al. 2014).

Subsequently, the ORR performances of all the samples were accurately investigated by detailed electrochemical tests. Cyclic voltammetry (CV) curves in N_2- and O_2-saturated 0.1 M KOH, respectively, of all the catalysts, were first used to investigate the ORR performance of all catalysts. As shown in Fig. 5a, it was self-evident that there were oxygen reduction current peaks for all the samples appearing in the O_2-saturated electrolyte, whereas in the N_2-saturated electrolyte, there was no obvious oxygen reduction current peak. The ORR peak potential of FeCo/N-C CNFs is ~ 0.83 V which is close to the Pt/C (0.90 V) and more positive than that for Fe/N-C CNFs (0.76 V) and Co/N-C CNFs (0.71 V),

indicating that FeCo/N-C CNFs shows the good ORR performance. Meantime, from the CV curves obtained in N_2-saturated 0.1 M KOH, the double-layer capacitance of FeCo/N-C CNF catalysts was much higher than of other contrast samples, suggesting FeCo/N-C CNF catalysts had a larger solid-electrolyte interface due to their higher BET surface areas. Electrochemical impedance spectroscopy (EIS) measurements were conducted to investigate the electroconductivity of FeCo/N-C CNFs, Fe/N-C CNFs, and Co/N-C CNFs. As shown in Figure S2 and Table S1, it can been seen that CoFe/N-C CNFs exhibit the lower charge-transfer resistance (R_{ct} = 27.52 Ω) than Co/N-C CNFs (R_{ct} = 37.71 Ω), Fe/N-C CNFs(R_{ct} = 33.90 Ω), indicating that CoFe/N-C CNFs had the highest electron conductive ability among them (Gao et al. 2017 and He et al. 2017). Further, linear sweep voltammetry (LSV) is used to investigate the ORR performance of the catalysts. As revealed in Fig. 5b, FeCo/N-C CNFs display a satisfactory Pt/C like ORR activity. Although the half-wave potential ($E_{1/2}$, 0.834 V) and onset potential
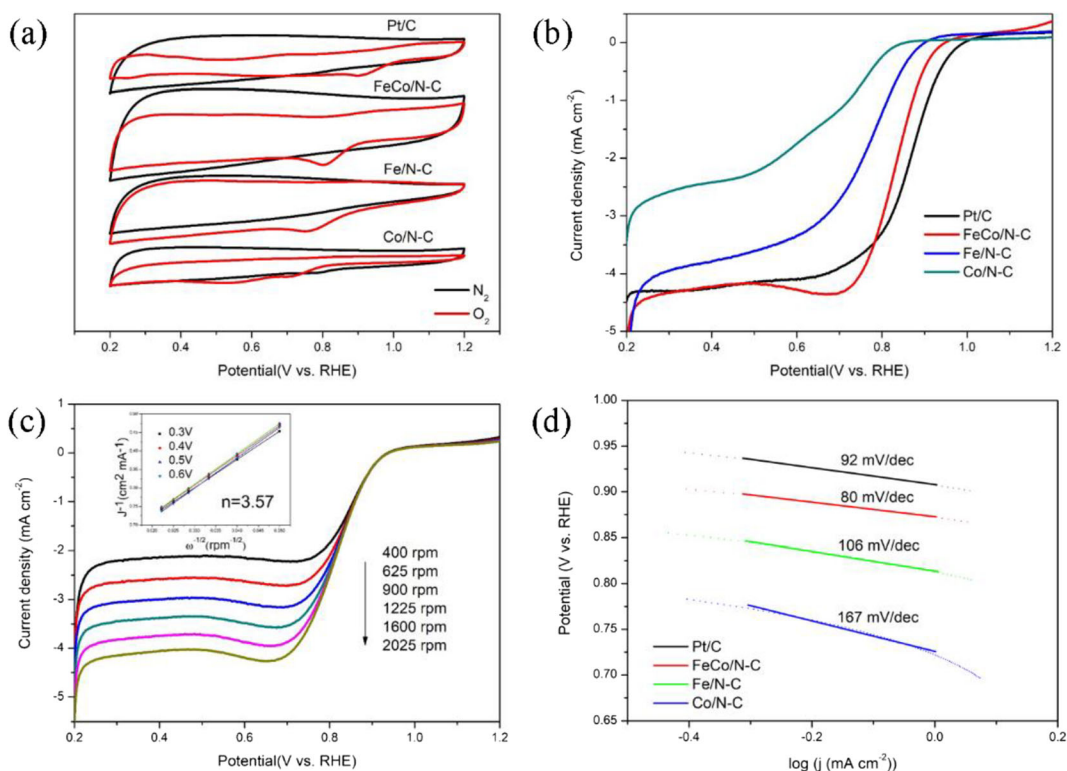
Fig. 5 **a** CV curves in N_2- or O_2-saturated 0.1 M KOH solution of Pt/C, FeCo/N-C CNF, Fe/N-C CNF, and Co/N-C CNF catalysts (scan rate 50 mV s^{-1}). **b** ORR LSV curves of Pt/C, FeCo/N-C CNFs, Fe/N-C CNFs, and Co/N-C CNFs catalysts. **c** LSV curves of FeCo/N-C CNFs at different rotation speeds (inset figure is the K-L plots of FeCo/N-C CNFs with different electrode potentials). **d** Tafel plots of Pt/C, FeCo/N-C CNF, Fe/N-C CNF, and Co/N-C CNF catalysts

(E_{onset}, 0.990 V) of FeCo/N-C CNFs are more negative than Pt/C (0.863 V, 1.034 V), the limiting current density (4.33 mA cm^{-2}) is comparable to commercial 20% Pt/C (4.20 mA cm^{-2}), moreover, which outperforms that of the other two contrast catalysts.

To investigate the kinetics mechanism of the ORR during the reaction, we recorded the ORR polarization curves of FeCo/N-C CNFs (Fig. 5c) and commercial Pt/C at various rotation speeds (400−2025 rpm). Higher rotational speed reduces the diffusion distance and
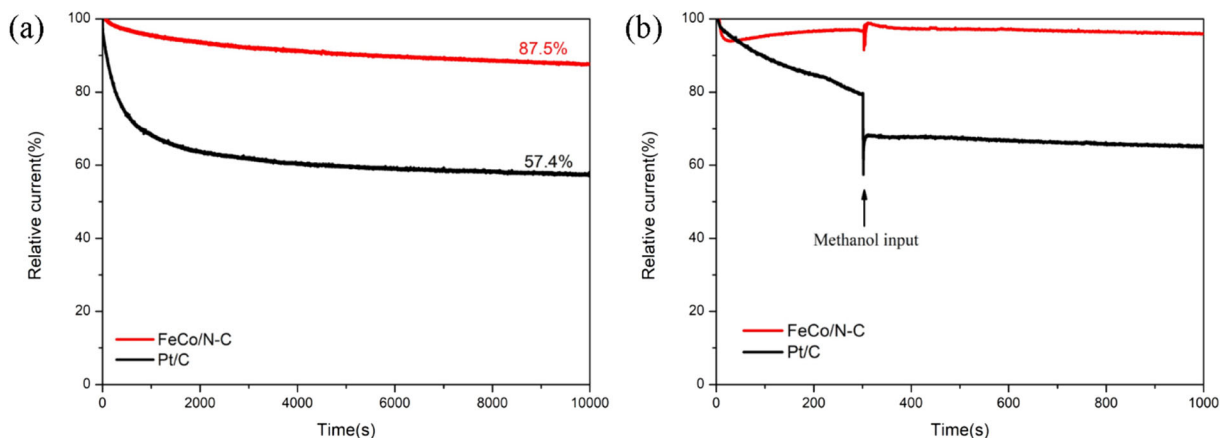
Fig. 6 **a** Electrochemical stability test. **b** Methanol tolerance test by current-time curves of FeCo/N-C CNFs and 20% Pt/C at 0.65 V in O_2-saturated 0.1 M KOH at 1600 rpm

further increase the current density. According to the Koutecky-Levich (K-L) equation, we can calculate the electron transfer number (n). The corresponding K–L plots of FeCo/N-C CNFs (inset of Fig. 5c) and commercial Pt/C exhibit good linear correlation indicating the first-order reaction kinetics toward the dissolved oxygen concentration (Liang et al. 2011). From the inset K–L plot in Fig. 5c, the slope of the K–L plot is about ~ 3.57 ranging from + 0.3 to + 0.6 V which is close to an ideal four-electron pathway (n = 4), meaning that the FeCo/N-C CNFs can catalyze a 4-electron oxygen reduction reaction (Xu et al. 2017 and Chai et al. 2019). Determined from electrochemical double-layer capacitance (C_{dl}) (Nai et al. 2018 and Deng et al. 2016), the electrochemically active surface areas (ECSAs) of FeCo/N-C CNFs is about 145 cm^{-2} (Supporting information). Moreover, the corresponding Tafel plots are shown in Fig. 5d the FeCo/N-C CNFs were observed a Tafel plot slope of 80 mV dec^{-1}, which was smaller than that of commercial Pt/C (92 mV dec^{-1}), Fe/N-C CNFs (106 mV dec^{-1}), and Co/N-C CNFs (167 mV dec^{-1}). Based on the above observations, the FeCo/N-C CNFs had a more superior electron transfer rate and kinetic reaction than the other three catalyst samples.

Besides the ORR activity of catalysts, we also tested its methanol tolerance and long-term stability. The methanol tolerance test was investigated by chronoamperometry with injection of a certain amount of methanol into the electrolyte at a specific time. The long-term stability performance was also investigated by chronoamperometric measurements (Fig. 6a). After the electrochemical stability test for 10,000 s at 1600 rpm, about 87.5% of the initial current density can be maintained, which is a lot better than that for Pt/C (59.4%), suggesting the excellent stability of FeCo/N-C CNFs. From Fig. 6b, after injecting methanol, we can see there was no apparent fluctuation of current density for FeCo/N-C CNFs, while an obvious current density reduction for the Pt/C could be observed, suggesting the better tolerance performance of FeCo/N-C CNFs to crossover effect.

Conclusion

In general, the porous FeCo/N-C CNF electrocatalysts were successfully fabricated by using electrospinning, immersion, and simple pyrolysis. In the process of immersion, the ZnCo-ZIF can be generated on the surfaces of the electrospun composite fibers, facilitating the formation of interconnected porous structure in pyrolysis. The porous FeCo/N-C CNFs catalysts exhibited high ORR performance. Remarkably, in alkaline media, the FeCo/N-C CNFs exhibited a satisfactory Pt/C like ORR activity. It is also proved that FeCo/N-C CNFs displayed not only more outstanding long-time durability but also methanol crossover effect tolerance than those of commercial Pt/C in alkaline solution. The high ORR catalytic performances of FeCo/N-C CNF catalysts are mainly derived from the following important aspects: (i) the doping Fe, Co, and N led to inhomogeneous charge distribution which facilitates the capture of oxygen species by the catalysts during the reaction (Tong et al. 2017; Wang et al. 2017; Gong et al. 2009); (ii) the porous structure gives a large specific surface area, derived from etching by Zn^{2+} in the fiber, improving the stability of the reaction and accelerates mass transport of reactants; and (iii) the doping of Fe-N$_x$ and Co-N$_x$ enhances the electron transfer ability and acts as an ORR active site (Tan et al. 2018; Wu et al. 2012; Zhou et al. 2017; Meng et al. 2016). The outcomes of this study may bring some new synthesis strategy for the preparation of non-precious carbon-based electrocatalyst and have a high potential for fuel cells.

Compliance with ethical standards

Conflict of Interest The authors declare that they have no conflict of interest.

References

Alegre C, Busacca C, Di Blasi O, Antonucci V, Aricò AS, Di Blasi A, Baglio V (2017) A combination of CoO and Co nanoparticles supported on electrospun carbon nanofibers as highly stable air electrodes. J Power Sources 364:101–109. https://doi.org/10.1016/j.jpowsour.2017.08.007

An L, Jiang N, Li B, Hua S, Fu Y, Liu J, Hao W, Xia D, Sun Z (2018) A highly active and durable iron/cobalt Alloy catalyst encapsulated in N-doped graphitic carbon nanotubes for oxygen reduction reaction by a nanofibrous dicyandiamide template. J Mater Chem A 6:5962–5970. https://doi.org/10.1039/C8TA01247D

Chen YZ, Wang C, Wu ZY, Xiong Y, Xu Q, Yu SH, Jiang HL (2015) From bimetallic metal-organic framework to porous carbon: high surface area and multicomponent active dopants for excellent electrocatalysis. Adv Mater 27:5010–5016. https://doi.org/10.1002/adma.201502315

Chen Y, Li X, Park K, Lu W, Wang C, Xue W, Yang F, Zhou J, Suo L, Lin T, Huang H, Li J, Goodenough JB (2017) Nitrogen-doped carbon for sodium-ion battery anode by self-etching and graphitization of bimetallic MOF-based composite. Chem 3:152–163. https://doi.org/10.1016/j.chempr.2017.05.021

Chai L, Zhang L, Wang X, Xu L, Han C, Li TT, Hu Y, Qian J, Huang S (2019) Bottom-up synthesis of MOF-derived hollow N-doped carbon materials for enhanced ORR performance. Carbon 146:248–256. https://doi.org/10.1016/j.carbon.2019.02.006

Deng H, Zhang C, Xie Y, Tumlin T, Giri L, Karna SP, Lin J (2016) Laser induced MoS_2/carbon hybrids for hydrogen evolution reaction catalysts. J Mater Chem A 4(18):6824–6830. https://doi.org/10.1039/C5TA09322H

Deng J, Yu L, Deng D, Chen X, Yang F, Bao X (2013) Highly active reduction of oxygen on A FeCo alloy catalyst encapsulated in pod-like carbon nanotubes with fewer walls. J Mater Chem A 1:14868. https://doi.org/10.1039/C3TA13759G

Dresselhaus MS, Thomas IL (2001) Alternative energy technologies. Nature 414:332–337. https://doi.org/10.1038/35104599

Gao S, Fan B, Feng R, Ye C, Wei X, Liu J, Bu X (2017) N-doped-carbon-coated Fe_3O_4 from metal-organic framework as efficient electrocatalyst for ORR. Nano Energy 40:462–470. https://doi.org/10.1016/j.nanoen.2017.08.044

Gong K, Du F, Xia Z, Durstock M, Dai L (2009) Nitrogen-doped carbon nanotube arrays with high electrocatalytic activity for oxygen reduction. Science 323:760–764. https://doi.org/10.1126/science.1168049

Guan BY, Lu Y, Wang Y, Wu M, Lou XWD (2018) Porous iron-cobalt alloy/nitrogen-doped carbon cages synthesized via pyrolysis of complex metal-organic framework hybrids for oxygen reduction. Adv Funct Mater 28:1706738. https://doi.org/10.1002/adfm.201706738

Guo Y, Yuan P, Zhang J, Hu Y, Amiinu IS, Wang X, Zhou J, Xia H, Song Z, Xu Q, Mu S (2018) Carbon nanosheets containing discrete Co-Nx-By-C active sites for efficient oxygen electrocatalysis and rechargeable Zn-air batteries. ACS Nano 12:1894–1901. https://doi.org/10.1021/acsnano.7b08721

Guruvammal D, Selvaraj S, Meenakshi Sundar S (2016) Effect of Ni-doping on the structural, optical and magnetic properties of ZnO nanoparticles by solvothermal method. J Alloys Compd 682:850–855. https://doi.org/10.1016/j.jallcom.2016.05.038

He D, Xiong Y, Yang J, Chen X, Deng Z, Pan M, Li Y, Mu S (2017) Nanocarbon-intercalated and Fe–N-codoped graphene as a highly active noble-metal-free bifunctional electrocatalyst for oxygen reduction and evolution. J Mater

Chem A 5(5):1930–1934. https://doi.org/10.1039/C5TA09232A

Hou H, Jun Z, Weller F, Greiner A (2003) Large-scale synthesis and characterization of helically coiled carbon nanotubes by use of $Fe(CO)_5$ as floating catalyst precursor. Chem Mater 15:3170–3175. https://doi.org/10.1021/cm021290g

Hu E, Yu XY, Chen F, Wu Y, Hu Y, Lou XWD (2017) Graphene layers-wrapped Fe/Fe_5C_2 nanoparticles supported on N-doped graphene nanosheets for highly efficient oxygen reduction. Adv Energy Mater 8:1702476. https://doi.org/10.1002/aenm.201702476

Jaouen F, Proietti E, Lefèvre M, Chenitz R, Dodelet JP, Wu G, Chung HT, Johnston CM, Zelenay P (2011) Recent advances in non-precious metal catalysis for oxygen-reduction reaction in polymer electrolyte fuel cells. Energy Environ Sci 4:114–130. https://doi.org/10.1039/c0ee00011f

Jiang S, Zhu C, Dong S (2013) Cobalt and nitrogen-cofunctionalized graphene as a durable non-precious metal catalyst with enhanced ORR activity. J Mater Chem A 1:3593. https://doi.org/10.1039/C3TA01682J

Lee CJ, Park J, Yu JA (2002) Catalyst effect on carbon nanotubes synthesized by thermal chemical vapor deposition. Chem Phys Lett 360:250–255. https://doi.org/10.1016/S0009-2614(02)00831-X

Lefevre M, Proietti E, Jaouen F, Dodelet JP (2009) Iron-based catalysts with improved oxygen reduction activity in polymer electrolyte fuel cells. Science 324:71–74. https://doi.org/10.1126/science.1170051

Li Y, Gong M, Liang Y, Feng J, Kim JE, Wang H, Hong G, Zhang B, Dai H (2013) Advanced zinc-air batteries based on high-performance hybrid electrocatalysts. Nat Commun 4:1805. https://doi.org/10.1038/ncomms2812

Liang HW, Wei W, Wu ZS, Feng X, Mullen K (2013) Mesoporous metal-nitrogen-doped carbon electrocatalysts for highly efficient oxygen reduction reaction. J Am Chem Soc 135:16002–16005. https://doi.org/10.1021/ja407552k

Liang Y, Li Y, Wang H, Zhou J, Wang J, Regier T, Dai H (2011) Co_3O_4 nanocrystals on graphene as a synergistic catalyst for oxygen reduction reaction. Nat Mater 10:780–786. https://doi.org/10.1126/10.1038/nmat3087

Lin L, Zhu Q, Xu AW (2014) Noble-metal-free Fe-N/C catalyst for highly efficient oxygen reduction reaction under both alkaline and acidic conditions. J Am Chem Soc 136:11027–11033. https://doi.org/10.1021/ja504696r

Liu R, Wu D, Feng X, Mullen K (2010) Nitrogen-doped ordered mesoporous graphitic arrays with high electrocatalytic activity for oxygen reduction. Angew Chem Int Ed 49:2565–2569. https://doi.org/10.1002/ange.200907289

Lu B, Smart TJ, Qin D, Lu JE, Wang N, Chen L, Peng Y, Ping Y, Chen S (2017) Nitrogen and iron-codoped carbon hollow nanotubules as high-performance catalysts toward oxygen reduction reaction: a combined experimental and theoretical study. Chem Mater 29:5617–5628. https://doi.org/10.1021/acs.chemmater.7b01265

Mahmood J, Li F, Kim C, Hj C, Gwon O, Jung SM, Seo JM, Cho SJ, Ju YW, Jeong HY, Kim G, Baek JB (2018) $Fe@C_2N$: a highly-efficient indirect-contact oxygen reduction catalyst. Nano Energy 44:304–310. https://doi.org/10.1016/j.nanoen.2017.11.057

Meng F, Zhong H, Bao D, Yan J, Zhang X (2016) In situ coupling of strung Co_4N and intertwined N-C fibers toward free-

standing bifunctional cathode for robust, efficient, and flexible Zn-air batteries. J Am Chem Soc 138:10226–10231. https://doi.org/10.1021/jacs.6b05046

Nai J, Zhang J, Lou XW (2018) Construction of single-crystalline Prussian blue analog hollow nanostructures with tailorable topologies. Chem 4(8):1967–1982. https://doi.org/10.1016/j.chempr.2018.07.001

Peng H, Mo Z, Liao S, Liang H, Yang L, Luo F, Song H, Zhong Y, Zhang B (2013) High performance Fe- and N-doped carbon catalyst with graphene structure for oxygen reduction. Sci Rep 3:1765–1772. https://doi.org/10.1038/srep01765

Qiu Y, Yu J, Shi T, Zhou X, Bai X, Huang JY (2011) Nitrogen-doped ultrathin carbon nanofibers derived from electrospinning: large-scale production, unique structure, and application as electrocatalysts for oxygen reduction. J Power Sources 196:9862–9867. https://doi.org/10.1016/j.jpowsour.2011.08.013

Qu L, Liu Y, Baek JB, Dai L (2010) Nitrogen-doped graphene as efficient metal-free electrocatalyst for oxygen reduction in fuel cells. ACS Nano 4:1321–1326. https://doi.org/10.1021/nn901850u

Shanmugam S, Osaka T (2011) Efficient electrocatalytic oxygen reduction over metal free-nitrogen doped carbon nanocapsules. Chem Commun 47:4463–4465. https://doi.org/10.1039/C1CC10361J

Singh KP, Bae EJ, Yu JS (2015) Fe-P: a new class of electroactive catalyst for oxygen reduction reaction. J Am Chem Soc 137:3165–3168. https://doi.org/10.1021/ja511759u

Su CY, Cheng H, Li W, Liu ZQ, Li N, Hou Z, Bai FQ, Zhang HX, Ma TY (2017) Atomic modulation of FeCo-nitrogen-carbon bifunctional oxygen electrodes for rechargeable and flexible all-solid-state zinc-air battery. Adv Energy Mater 7: 1602420. https://doi.org/10.1002/aenm.201602420

Tan M, He T, Liu J, Wu H, Li Q, Zheng J, Wang Y, Sun Z, Wang S, Zhang Y (2018) Supramolecular bimetallogels: a nanofiber network for bimetal/nitrogen Co-doped carbon electrocatalysts. J Mater Chem A 6:8227–8232. https://doi.org/10.1039/C8TA01898G

Tong Y, Chen P, Zhou T, Xu K, Chu W, Wu C, Xie Y (2017) A bifunctional hybrid electrocatalyst for oxygen reduction and evolution: cobalt oxide nanoparticles strongly coupled to B, N-decorated graphene. Angew Chem Int Ed 56:7121-7125. https://doi.org/10.1002/ange.201702430

Wang B (2005) Recent development of non-platinum catalysts for oxygen reduction reaction. J Power Sources 152:1–15. https://doi.org/10.1016/j.jpowsour.2005.05.098

Wang H, Keum JK, Hiltner A, Baer E, Freeman B, Rozanski A, Galeski A (2009) Confined crystallization of polyethylene oxide in nanolayer assemblies. Science 323:757–760. https://doi.org/10.1126/science.1164601

Wang H, Wang W, Asif M, Yu Y, Wang Z, Wang J, Liu H, Xiao J (2017) Cobalt ion-coordinated self-assembly synthesis of nitrogen-doped ordered mesoporous carbon nanosheets for efficiently catalyzing oxygen reduction. Nanoscale 9:15534–15541. https://doi.org/10.1039/C7NR05208A

Wu T, Fan J, Li Q, Shi P, Xu Q, Min Y (2018) Palladium nanoparticles anchored on anatase titanium dioxide-black phosphorus hybrids with heterointerfaces: highly electroactive and durable catalysts for ethanol electrooxidation. Adv Energy Mater 8:1701799. https://doi.org/10.1002/aenm.201701799

Wu ZS, Yang S, Sun Y, Parvez K, Feng X, Mullen K (2012) 3D nitrogen-doped graphene aerogel-supported Fe_3O_4 nanoparticles as efficient electrocatalysts for the oxygen reduction reaction. J Am Chem Soc 134:9082–9085. https://doi.org/10.1021/ja3030565

Xu S, Kim Y, Higgins D, Yusuf M, Jaramillo TF, Prinz FB (2017) Building upon the Koutecky-Levich equation for evaluation of next-generation oxygen reduction reaction catalysts. Electrochim Acta 255:99–108. https://doi.org/10.1016/j.electacta.2017.09.145

Yamashita T, Hayes P (2008) Analysis of XPS spectra of Fe^{2+} and Fe^{3+} ions in oxide materials. Appl Surf Sci 254:2441–2449. https://doi.org/10.1016/j.apsusc.2007.09.063

Yang L, Zeng X, Wang W, Cao D (2018) Recent progress in MOF-derived, heteroatom-doped porous carbons as highly efficient electrocatalysts for oxygen reduction reaction in fuel cells. Adv Funct Mater 28:1704537. https://doi.org/10.1002/adfm.201704537

Yang W, Liu X, Chen L, Liang L, Jia J (2017) A metal-organic framework devised Co-N doped carbon microsphere/nanofiber hybrid as a free-standing 3D oxygen catalyst. Chem Commun 53:4034-4037.https://doi.org/10.1039/C7CC01349C

Yang W, Liu X, Yue X, Jia J, Guo S (2015) Bamboo-like carbon nanotube/Fe_3C nanoparticle hybrids and their highly efficient catalysis for oxygen reduction. J Am Chem Soc 137:1436–1439. https://doi.org/10.1021/ja5129132

Zhang C, Liu J, Ye Y, Aslam Z, Brydson R, Liang C (2018a) Fe-N-doped mesoporous carbon with dual active sites loaded on reduced graphene oxides for efficient oxygen reduction catalysts. ACS Appl Mater Interfaces 10:2423–2429. https://doi.org/10.1021/acsami.7b14443

Zhang G, Lu W, Cao F, Xiao Z, Zheng X (2016) N-doped graphene coupled with Co nanoparticles as an efficient electrocatalyst for oxygen reduction in alkaline media. J Power Sources 302:114–125. https://doi.org/10.1016/j.jpowsour.2015.10.055

Zhang Y, Lin Y, Jiang H, Wu C, Liu H, Wang C, Chen S, Duan T, Song L (2018b) Well-defined cobalt catalyst with N-doped carbon layers enwrapping: the correlation between surface atomic structure and electrocatalytic property. Small 14: 1702074. https://doi.org/10.1002/smll.201702074

Zhao Y, Lai Q, Wang Y, Zhu J, Liang Y (2017) Interconnected hierarchically porous Fe, N-codoped carbon nanofibers as efficient oxygen reduction catalysts for Zn-air batteries. ACS Appl Mater Interfaces 9:16178–16186. https://doi.org/10.1021/acsami.7b01712

Zhou B, Liu L, Cai P, Zeng G, Li X, Wen Z, Chen L (2017) Ferrocene-based porous organic polymer derived high-performance electrocatalysts for oxygen reduction. J Mater Chem A 5:22163–22169. https://doi.org/10.1039/C7TA06515A

Zhu H, Zhang S, Su D, Jiang G, Sun S (2015) Surface profile control of FeNiPt/Pt core/shell nanowires for oxygen reduction reaction. Small 11:3545–3549. https://doi.org/10.1002/smll.201500330